PFC/JA-87-34

Access to the Second Stability Region in a High Shear, Low Aspect Ratio Tokamak

Gerver, M.J.; Kesner, J.; Ramos, J.J.

July 1988

Plasma Fusion Center
Massachusetts Institute of Technology
Cambridge, MA 02139 USA

Submitted for publication in: Physics of Fluids

To be published in Physics of Fluids

PFC/JA-87-34

Access to the Second Stability Region in a High Shear, Low Aspect Ratio Tokamak

M.J. Gerver, J. Kesner, J.J. Ramos

Massachusetts Institute of Technology

Cambridge , Massachusetts

ABSTRACT

It is known that tokamaks display a second region of stability to ideal magnetohydrodynamic (MHD) internal modes. An important determining factor for MHD properties is the radial profile of toroidal current. Here it is shown that in a low aspect ratio tokamak with high on-axis safety factor ($q_0 \simeq 2$) and high shear a path to high beta can be obtained that remains completely stable against ideal MHD modes. By maintaining high shear this scenario avoids fixed boundary instabilities for both high and low toroidal mode numbers for beta values well above the Troyon limit (stability was tested up to $\epsilon\beta_p = 1.4$, $\beta = 10.8\%$). For a close fitting wall ($a_{wall}/a_{plasma} \simeq 1.2$) this configuration is also stable to low toroidal mode number balloon-kink modes.

I. INTRODUCTION

High beta is desirable in fusion devices, and beta limitations imposed by ideal magnetohydrodynamics (MHD) have been the subject of active research for tokamak confinement devices. Although MHD pressure driven modes usually impose a severe constraint in tokamaks, it has been shown that at sufficiently high beta these devices can exhibit second regions of stability to high-n ballooning modes (where n is the toroidal mode number)[1−6]. Generally there is an unstable gap at intermediate beta separating the first and second stability regions.

In order to obtain high beta in an actual experiment one would like to eliminate the unstable region that separates the so-called "second stability region" from the first region. In this work we demonstrate a method of achieving this result through the use of current profile control [7−11]to raise the on-axis safety factor q_o in a low aspect ratio torus. This can be accomplished , for example, using RF or neutral beam current drive.

Previous studies of stable access to the second stability region have either raised the on-axis safety factor [7,8,11−13], used indentation[14] , or some combination of profile shaping and indentation [15,16]. Attempts to bridge the unstable region through the use of hot electrons were also considered [17−19]. For all of the non-indented configurations a low shear profile was used. In these cases, it is possible that the global shear, s (defined later) may fall significantly below unity at the flux surface with the maximum pressure gradient, and this, in turn, might drive unstable low-n, fixed boundary instabilities, termed "infernal" modes [20]. In this article, we report for the first time a completely stable access path to the second stability region without indentation while maintaining $q_e/q_0 \approx 4$ and $s > 1$ over most of the plasma profile.

Aspect ratio and toroidal current profile are an important determinant for MHD stability. Theoretical analyses that utilize a large aspect ratio expansion cannot properly predict low aspect ratio scaling. Codes such as PEST [21] which permit arbitrary aspect ratio must be utilized in these studies.

We have found that low aspect ratio is favored for entrance into the high beta (second stability) tokamak operating regime. The reasons are as follows:

1. At low aspect ratio a reduction in the local shear is produced at the outside of the torus at low beta. (For large aspect ratio shaping or finite beta is required to produce such an effect).

2. High q_0 improves the average good curvature of the torus and this effect is amplified by low aspect ratio.

In section 2 we review the physical mechanisms that produce the second stability region and discuss the different approaches to it. Here we will explain the stabilizing influence of combining low aspect ratio with high q. Section 3 displays numerical calculations of an illustrative example of a low aspect ratio, high q, high shear tokamak. Section 4 contains our conclusions.

II. SECOND STABILITY: THEORETICAL CONSIDERATIONS

In axisymmetric configurations like a tokamak, the equilibrium magnetic field can be represented as

$$\mathbf{B} = \nabla\psi \times \nabla\alpha = \nabla\psi \times \nabla\varphi + g(\psi)\nabla\varphi \tag{1}$$

with

$$\alpha = \varphi - \int_{\theta_0}^{\theta} \frac{\mathbf{B}\cdot\nabla\varphi}{\mathbf{B}\cdot\nabla\theta} d\theta. \tag{2}$$

Here $2\pi\psi$ is the poloidal flux, φ is the toroidal angle and θ is a poloidal coordinate. The equilibrium condition $\mathbf{j}\times\mathbf{B} = \nabla p$ with $\mathbf{j} = \nabla\times\mathbf{B}$ leads to the Grad-Shafranov equation:

$$\nabla\cdot\left(R^{-2}\nabla\psi\right) = \mathbf{j}\cdot\nabla\varphi = -\frac{dp}{d\psi} - \frac{g}{R^2}\frac{dg}{d\psi} \tag{3}$$

where R is the distance from the axis of symmetry. We shall use the following definition of volume averaged poloidal beta, β_p ,

$$\beta_p \equiv \frac{4 < p >}{R_0 I_p^2}$$

with $< p >= \int p \, dV$.

High-n ballooning modes at marginal stability are described by the following equation [22–24]:

$$\mathbf{B}\cdot\nabla\left(\frac{|\nabla\alpha|^2}{B}\mathbf{B}\cdot\nabla F\right) + \frac{2}{|\nabla\psi|}\frac{dp}{d\psi}\left(\kappa_n + \kappa_g\frac{I|\nabla\psi|^2}{B^2}\right)F = 0 \tag{4}$$

where F is the ballooning eigenfunction and κ_n and κ_g are the normal and geodesic components of the magnetic curvature: $\boldsymbol{\kappa} = (\hat{e}_B \cdot \nabla)\, \hat{e}_B = \kappa_n \hat{e}_\psi + \kappa_g \hat{e}_\psi \times \hat{e}_B$, $\hat{e}_\psi$ and $\hat{e}_B$ being the unit vectors in the directions of $\nabla\psi$ and $\mathbf{B}$. Also

$$|\nabla\alpha|^2 = \frac{B^2}{|\nabla\psi|^2} + |\nabla\psi|^2 I^2 \tag{5}$$

with

$$I \equiv -\frac{\nabla\alpha \cdot \nabla\psi}{|\nabla\psi|^2} = \frac{1}{|\nabla\psi|^2} \nabla\psi \cdot \nabla \left[\int_{\theta_0}^{\theta} \frac{\mathbf{B} \cdot \nabla\varphi}{\mathbf{B} \cdot \nabla\theta} d\theta \right] \tag{6}$$

Since $(\mathbf{B} \cdot \nabla\varphi) \,/\, (\mathbf{B} \cdot \nabla\theta) = q_\ell$ represents the local pitch of the magnetic field lines, the quantity I represents the integrated local shear. The first term in Eq. (4) contains the stabilizing effects of field line bending and shear. Notice that the magnetic shear enters through the square of the integrated function I. The second term, proportional to $dp/d\psi$, contains the ballooning drive that results from the combined effects of pressure gradient and magnetic curvature. It involves a part proportional to the normal curvature κ_n and a part proportional to the geodesic curvature κ_g. The latter is coupled to the integrated local shear function I, this being a consequence of the short perpendicular wavelength nature of the high-n modes under consideration.

A stable entrance into the second stability region requires a combination of effects brought about by the high-beta equilibrium, that decrease the strength of the instability driving forces while enhancing the restoring forces. Three such effects are clearly identifiable.

1. The strengthening of the poloidal field on the outer side of the torus that results from the large outward shift of the magnetic surfaces characteristic of high-beta equilibria. This shortens the "connection length" or distance along a magnetic field line within the region of unfavorable curvature. This stabilizing effect diminishes the instability drive associated with the normal curvature and enhances the stabilizing force associated with the magnetic tension, acting equally on low and high toroidal mode number modes [1-6,25-27].

2. The reversal of the local magnetic shear on the outside of the torus. This has the net effect of stabilizing the region where the ballooning mode will ordinarily localize since the destabilizing normal curvature is maximum there[1-6]. In a low aspect ratio torus geometric effects will decrease the local shear on the outside of the torus and thus facilitate shear reversal. This effect is only relevant to high-n modes.

3. The enhancement of the region of favorable magnetic curvature [7,8,11] brought about by toroidal effects in configurations with small aspect ratio and large values of the inverse rotational number q. This effect is present at all beta values.

We shall exploit all of these effects in order to achieve a stable path from the first to the second stability regimes. In the following sections we will discuss in some detail these three stabilizing processes.

A. Local strengthening of the poloidal field

In high-beta tokamaks, the large outward force acting on the confined plasma is balanced by strengthening the poloidal field on the outer side of the torus, where the distance from the axis of symmetry is largest. This is due to the significant outward shift of the magnetic axis that compresses the magnetic surfaces and gives rise to larger values of $|\nabla\psi|$ or B_p on the outer side of the torus relative to those on the inner side. For vertically (up-down) symmetric configurations, the normal curvature κ_n is an even function of the poloidal angle, (roughly proportional to $\cos\theta$ for large aspect ratio circular tokamaks) with unfavorable (destabilizing) sign on the outer side and favorable (stabilizing) sign on the inner side. As shown by Eq. (4) the instability driving term associated with κ_n appears divided by $|\nabla\psi|$. At low beta, $|\nabla\psi| = RB_p$ can be assumed to be a nearly constant function of the poloidal angle. However, as discussed before, at high beta $|\nabla\psi|$ is considerably enhanced in the region of unfavorable curvature, thus the instability drive of the normal curvature is depressed. In fact this instability driving term is effectively depressed by a further power of $|\nabla\psi|$ because the derivatives in the (shear-Alfvén) first term of Eq. (4) are taken along the magnetic field line. This is the so called the "shortening of the connection length" stabilizing effect. Figure 1 illustrates these properties. In a low-beta equilibrium with nearly uniform poloidal field, a magnetic field line spends almost equal lengths in the favorable and unfavorable regions. On the contrary, for a high-beta equilibrium with enhanced poloidal component in the unfavorable curvature region, the magnetic field line length in this region is reduced.

Low-n modes are mostly driven by the normal component of the magnetic curvature that aligns itself with the pressure gradient (provided $q_0 \geq 1$). Therefore the stabilizing effect discussed in this section applies equally to low-n modes and is responsible for the existence of the second stability region also at low toroidal wavenumbers [25–28].

B. Local reversal of the magnetic shear

In tokamaks the average rotational transform decreases away from the magnetic axis, in other words the average shear defined by $s = \psi\, dq/d\psi$ is positive. In low-beta, high aspect ratio equilibria with nearly uniform poloidal fields around a magnetic surface, the local shear is also nearly uniform as a function of θ and has the same sign as its flux surface average. Therefore, the integrated local shear function I is monotonically increasing as illustrated in Fig. 2. However, high-beta equilibria tend to decrease locally the value of the shear on the outer side of the torus. For sufficiently high beta this local shear can change sign so that on the outer side, its sign is opposite to that of the average shear. (Shaping, and in particular indentation, will facilitate this effect.) This results in a locally decreasing integrated shear I as shown also in Fig. 2.

The geodesic curvature κ_g is an odd function of the poloidal angle (roughly proportional to $\sin\theta$ in large aspect ratio circular tokamaks). It enters the high-n ballooning equation as a reflection of the fact that these high-n modes must propagate perpendicularly to the magnetic field to avoid large field-bending. In the ballooning equation the geodesic curvature is coupled to the local magnetic shear in such a way that κ_g appears multiplied by the integrated function I. If I is monotonic, the destabilizing force is maximized by choosing $\theta_0 = 0$ so that I is also an odd function of θ and the product $\kappa_g I$ has a destabilizing sign for any θ $(-\pi < \theta < \pi)$. Since the shear enters the stabilizing shear-Alfvén term through I^2, this term is minimized by localizing the mode near $\theta = 0$ where $I = 0$. Now, because the vicinity of $\theta = 0$ is also subject to the largest destabilizing contribution from the normal curvature, an instability may develop. This is the conventional picture of the ballooning mode at the first instability threshold.

Equilibrium changes that take place at sufficiently high poloidal beta can cause a completely different picture to emerge [6]. If I is a decreasing function of θ near $\theta = 0$ and the parameter θ_0 were still chosen to be zero, the geodesic curvature term $\kappa_g I$ would be stabilizing in the $\theta \simeq 0$ region. This is where the mode would otherwise tend to be localized because $I = 0$, hence the shear stabilization minimized, and the instability drive of the normal curvature maximized. To avoid this situation we may have to choose $\theta_0 \neq 0$, presumably in such a way that a zero of I coincides with its local minimum as illustrated in Fig. 2. The minimum of I is by definition the point where the local shear, s_l, vanishes. By localizing the mode near the locus of vanishing local shear we minimize the shear stabilization while obtaining a destabilizing contribution from the geodesic curvature. If this mode localization is not too close to the region of stabilizing normal curvature an instability may develop. However, if beta is so high that the zero of the local shear has moved close to the region of favorable normal curvature (which may have been enhanced by the shortening of the connection length or other effects), it may not be possible to construct an unstable mode. This process produces the second stability region for high n ballooning modes.

In high aspect ratio tori the local shear is a monotonically increasing function of flux at low beta . As beta is increased local shear decreases on the outside of the torus. Eventually the local shear will reverse at the outside of the torus, and thereafter further increases in beta become stabilizing. Local shear reversal can be enhanced by shaping or simply by reducing the global shear. These two processes do not depend strongly on aspect ratio and lend themselves to theoretical studies that exploit large aspect ratio expansions. Current profile control, however, is most effective in low aspect ratio tori where such expansions cannot be made.

Figure 3 shows contours of local shear for tori of different shape at a fixed global shear defined by $q_0 \simeq 2, q_e \simeq 8$ with q_e the outer edge q value. Figure 3a shows the contours for a circular cross section high aspect ratio torus (A = 20) at low poloidal beta ($\beta_p = 0.01$). Figure 3b shows these contours in a low poloidal beta torus with aspect ratio 3. We observe here a distortion of the circular contours signifying a decrease in local shear on the outside of the torus. The origin of this effect can be seen from the following considerations: We can write the local q as

$$q_\ell = \frac{rB_t}{RB_p} = \frac{r(RB_t)}{R(RB_p)} = \frac{r\ g(\psi)}{R|\nabla\psi|}. \tag{7}$$

For circular, low beta equilibrium this becomes

$$q_\ell = q(\psi)\frac{1-\Delta' cos(\theta)}{1+(r/R_0)cos(\theta)} \tag{8}$$

with Δ the Shafranov shift for the flux surface at radius r and $\Delta' = d\Delta/dr$. Since $\Delta \approx r^2/8R_0 + O(\epsilon\beta_p)$ (for a flat current profile [29]), where ϵ is the inverse aspect ratio, we can obtain s_ℓ at $\theta = 0$ and low β

$$s_\ell(\theta=0) \propto r\ dq_\ell/dr = rq'(\psi)\frac{1-r/4R_0}{(1+r/R_0)} - \frac{r}{R_0}q(\psi)\frac{1.25}{(1+r/R_0)^2} \tag{9}$$

From Eq. 9 we observe that at large aspect ratio, $s_\ell(\theta=0) = s(\psi)$, the global shear, but as the aspect ratio A decreases, an $O(1/A)$ term subtracts from the global shear at the outside of the torus. At the transition to second stability $\epsilon\beta_p \sim 1$, and an additional term proportional to $q'\epsilon\beta_p$ would appear in Eq. 9. Now the last term in Eq. 9 is smaller than the $q'\epsilon\beta_p$ term by an order ϵ. However for low aspect ratio $\epsilon \sim 0.3$ this term offers a $\gtrsim$ 30 % correction that can easily provide the margin required for stability.

In Fig 3c we maintain low beta and consider a D shaped plasma cross section (ellipticity $\kappa = 1.4$, triangularity $\delta = 0.3$). We maintain an aspect ratio of $A = 3$ (although shaping is not dependent on aspect ratio). We observe a further reduction in the local shear at the outside of the torus and the development a small shear reversed region, which is cross-hatched. As beta increases (Figure 3d) this region grows and the amplitude of the reversed shear increases.

For high-n modes the local reversal of the magnetic shear is the dominant mechanism producing the second stability region. As a matter of fact, the simplest model ballooning equation (sometimes referred to as the $s-\alpha$ model) includes this effect as its only high beta feature, and shows the existence of a second stability region [2-4]. Unfortunately the local shear-geodesic curvature effects are important only for high-n modes. Low-n modes, which may be the most relevant ones, are mostly driven by the normal curvature (provided $q_0 \geq 1$).

The adoption of a low global shear configuration greatly reduces the restoring forces associated with the magnetic shear with no benefits whatsoever for low-n modes. This gives rise to the so called infernal instabilities [20], or low-n pressure driven modes that can become unstable much before their high-n counterparts. However, we have seen that the reduction of local shear through low aspect ratio and shaping effects also facilitates the reversal of local shear . This permits maintenance of strong global shear and presents the best option for stabilizing both high and low-n modes.

C. High q at small aspect ratio

The stabilizing effects discussed in the two previous sections are beta-related effects which produce the second stability region. Here we turn to a stabilizing effect that is not directly beta-related but depends strongly on the aspect ratio as it reflects a purely toroidal feature. This is the toroidal modification of the magnetic curvature that results in an enhanced favorable region if q is greater than one. The relevance of this to our second stability approach is that it provides a means of bridging the first and second stability regimes, so that an instability-free path to high beta can be obtained [7]. To illustrate this effect we consider a circular flux surface tokamak. The normal component of the magnetic curvature is

$$\kappa_n = -\frac{B_t^2}{B^2}\frac{\cos\theta}{R} - \frac{B_p^2}{B^2 r}. \tag{10}$$

In the infinite aspect ratio limit κ_n tends to $-\cos\theta/R_0$ so that its average vanishes and the regions of favorable and unfavorable curvature are equivalent. At finite aspect ratio we must take into account two new contributions: the contribution of the poloidal field (second term on the right hand side of Eq. (10)) which is unfavorable everywhere but proportional to q^{-2}, and the toroidal corrections associated with the poloidal variation of R ($R = R_0 + r\cos\theta$) which are favorable. Keeping finite aspect ratio corrections to first order for $\beta_p = O(1)$, we have

$$\kappa_n = -\frac{\cos\theta}{R_0} + \frac{r}{R_0^2}\left(\cos^2\theta - \frac{1}{q^2}\right) \tag{11}$$

For sufficiently large q, the unfavorable contribution of the poloidal field is depressed and a net enhancement of the favorable region is obtained. Of course, this being a toroidal effect, a finite aspect ratio is needed for it to make any significant difference in the stability properties of the plasma.

Given the previous considerations we selected a relatively low aspect ratio ($A = 3$) , high q ($q_0 = 2$), tokamak as our way of investigating the access to the second stability region. We are mostly interested in the stability against finite-n modes which are the ones that will affect the macroscopic behavior of the plasma. For this reason we do not consider the low-shear approach which is only relevant to high-n modes and may be very detrimental to low-n modes. We choose a high-shear equilibrium ($q_0 \simeq 2,\ q_e \simeq 7.6$) that should have good shear stabilization and be free from infernal instabilities. Second stability is due to the combination of strengthening of the poloidal field associated with large Shafranov shifts (which applies to both low-n and high-n modes), and to local shear reversal. The high q and low aspect ratio allow the connection between first and second stability regimes so that we are able to produce sequences of equilibria which are completely free of instabilities into the second stability regime.

Since no instability is actually found, "second stability " is defined as the point where further increases in beta make the incremental MHD potential energy W more negative. This happens for $\epsilon\beta_p \gtrsim 0.7$. Since at low beta ($\epsilon\beta_p \lesssim 1$) β is proportional to ϵ for fixed $\epsilon\beta_p$,

$$\beta \sim \epsilon\,(\epsilon\beta_p)\,q_e^{-2}$$

higher beta is required to reach second stability at low aspect ratio. This unfavorable scaling is mitigated by its q_e^{-2} dependence . In fact our $\epsilon = 1/3$ equilibria reach second stability against high-n modes at relatively modest beta values; $\epsilon\beta_p \simeq 0.7$, $\beta \simeq 1.2\%$. Moreover the relatively small aspect ratio allows a significant first stability domain where the plasma can be started and from which progress towards higher beta regimes can gradually be attempted.

III. NUMERICAL RESULTS

A. Equilibrium

In our calculations we determine equilibrium and high n Mercier and ballooning stability by means of the PEST code [21]. The code is run in the fixed boundary mode using 40 angular grid points (in π radians) and 40 flux surfaces. In the sequences shown the plasma pressure is augmented in steps of about 20 %. The geometry of the plasma boundary is characterized by an aspect ratio $A = 3$ ($R_0 = 0.9\ m, a = 0.3\ m$), elongation $\kappa = 1.4$, and triangularity $\delta = 0.3$. The vacuum toroidal field is taken to be 1 T and the plasma current varies from 130 kA up to 280 kA (see Table 1). We consider a sequence of equilibria with increasing beta and a roughly invariant q-profile characterized by high q_0 ($q_0 = 2$) and high shear ($q_e \simeq 7.6$). We also require that the toroidal current density be a well behaved function in the sense that it has no sign reversals, it vanishes approximately at the plasma edge, and its flux surface average is monotonically decreasing. In order to achieve this we proceed in the following way:

At low beta ($\epsilon\beta_p \leq 0.7$ we specify analytically the current density profile as

$$j_\phi = -R\frac{dp}{d\psi} - \frac{1}{2R}\frac{dg^2}{d\psi}$$

with

$$p = p_0\left(1 - \hat{\psi}\right)^\gamma$$

$$\frac{g^2}{(R^2B_t^2)_{vacuum}} = 1 + \frac{2g_p}{\gamma}\left(1 - \hat{\psi}\right)^\gamma$$

and

$$\hat{\psi} = \frac{\psi - \psi_0}{\psi_e - \psi_0}.$$

The parameter g_p is adjusted to obtain the desired edge safety factor $q_e = 7.6$, and γ ($\gamma \geq 1.5$) is adjusted to obtain the desired $q_0 = 2$. As p_0 is varied we generate in this fashion a sequence of equilibria with increasing beta, approximately invariant q profile, and vanishing current density at the plasma edge.

At high values of beta we approach an equilibrium limit. To avoid this limit we switch to a flux conserving sequence. That is to say we freeze the pressure profile width parameter ($\gamma = 1.5$) as well as the q-profile, and continue generating the higher beta equilibria sequence specified by $p(\psi) = p_0 \left(1 - \hat{\psi}\right)^{1.5}$ and $q(\psi)$ which is read numerically from the last analytic current profile equilibria ($\epsilon\beta_p$=0.7). In this way we generate equilibria up to $\epsilon\beta_p = 1.4$ and volume averaged beta = 10.8% with well behaved current profiles.

Figures 4 and 5 display the poloidal flux and toroidal current density contour plots for representative equilibria states in this sequence. Figures 6 and 7 show the corresponding ohmic current (flux surface averaged $j_{\|}$) and q profiles.

Figure 8 shows the toroidal current density, pressure, and safety factor q, as a function of major radius at the median plane of the torus, $z = 0$, for our highest beta ($\beta = 10.8$ %) case. Notice that the toroidal current remains positive throughout the cross section slice.

A consequence of flux conservation is that toroidal current increases with poloidal beta. Thus the current that was fixed at 130 kA in the lowest beta part of the ramp-up increases up to 280 kA in the highest beta ($\beta = 10.8\%$) equilibrium.

B. Stability of High Toroidal Number Modes

We have tested the stability of the above described equilibria against high toroidal mode number interchange and ballooning modes. The $q_0 = 2$ equilibria are stable on all flux surfaces with regard to the Mercier criterion for interchange modes. The ballooning equation (4) is solved with a shooting code to obtain the critical $p' = \mathrm{d}p/\mathrm{d}\psi$ at each magnetic surface. The results presented below depend of course on the pressure, current and safety factor profiles that we chose so the trends illustrated are more important than the exact parameters required for stability (i.e. q_0 and shape).

Figure 9 shows the ballooning mode stability criterion $(1\text{-}p'_{crit}/p')_{max}$ vs. $\epsilon\beta_p$. The subscript *max* refers to the most unstable (or least stable) magnetic surface (the surface that maximizes $1\text{-}p'_{crit}/p'$), so that all surfaces are stable when this parameter is less than zero. The $q_0 = 2$ equilibrium sequence shown was stable on all flux surfaces with regard to ballooning modes as well as to Mercier modes. We observe that past $\epsilon\beta_p \approx 0.6$ ($\beta \approx 1.2$ %) stability improves with increasing beta . Thus the second stability regime is reached. (The small jump that occurs at $\epsilon\beta_p \approx 0.6$ in Fig. 9 reflects a change in poloidal grid that was made to facilitate the flux conserving calculation. The kink in the curve at $\epsilon\beta_p \approx 0.8$ reflects a jump in the location of the least stable flux surface.

Since the local shear is zero at a finite poloidal angle θ, attention must be paid to varying the parameter θ_0 (Eq. 6) in order to look for the most unstable mode. After checking this we find that stability is maintained throughout the sequence.

For comparison with the q_0=2 sequence, similar sequences with $q_0 = 1$, $q_e \approx 4$ ($I_p \approx 300$ kA) and q_0=1.5, $q_e \approx 6$ ($I_p \approx 225$ kA) were also generated. Fig. 9 indicates that the $q_0 = 1.5$ startup path must traverse an unstable region that occupies up to 17 % of the radial dimension. The $q_0 = 1$ sequence does not completely restabilize.

The requirements on current control as a function of higher aspect ratio are illustrated in Fig 10. Here we vary the aspect ratio and plot the required q_0 for a stable transition into the second stability region as a function of aspect ratio, keeping q_e fixed at 8. For example A=9 requires $q_0 = 5.3$ for a stable transition to occur. Clearly a higher aspect ratio would require a higher q_0, which presents a more stringent requirement on profile control and reduces the global shear. It should be kept in mind that these results indicate trends and the exact requirement on q_0 depends on the class of profiles chosen.

C. Stability of Low Toroidal Number Modes

Low toroidal number modes can become unstable in fixed boundary plasmas (i.e. for a conducting wall at the plasma boundary) when the shear is sufficiently weak [30,20]. These instabilities have been termed infernal modes. We have considered the stability of fixed boundary modes with $n < 4$ using the PEST-2 code [21]using 128 angular grid points, 201 flux surfaces and keeping approximately 30 poloidal modes.

Sequences were followed up to beta values well in excess of the MHD beta limit proposed by Troyon [31] . The "Troyon limit" is expressed as a critical beta value which, in MKS units is given by

$$\beta_T = \frac{3 \times 10^{-8} I_p}{a B_0}.$$

In our calculations the transition to second stability occurs at β= 1.2 % whereas the Troyon limit is β_T= 1.5 %. (The Troyon limit is however calculated for an optimum q_0 of ≈ 1.2 and it degrades at higher q_0 [31]).

At the high q_e used ($q_e = 7.6$) the code is not able to adequately resolve values of $n > 3$ since the number of poloidal Fourier harmonics required for convergence scales as nq_e. However, we know from the calculations discussed in the previous section that the high-n modes are stable. The fixed boundary $n = 1$ to 3 modes were seen to be stable at all of the beta values considered. As the wall moves away from the plasma surface internal modes can couple to external kink modes.

Figure 11 shows the stability of the $n = 1$ to 3 modes as a function of wall position. (The error bars in this figure connect the last stable and first unstable wall position tested as the wall position recedes from the plasma boundary.) The modes reach their most unstable point indicated by the close required wall position, at about $\epsilon\beta_p \approx 1$ and then become more stable at higher beta. At high poloidal beta the $n = 2$ mode is more unstable than $n = 1$ because wall stabilization is weaker for this mode. The $n = 3$ mode is only slightly more unstable than $n = 2$ indicating that the expected stability of high-n modes (shown in the previous section) is beginning to appear. Moreover, because of the adopted high shear, and reasonable pressure profile the oscillatory dependence of the growth rate as a function of n, characteristic of infernal instabilities [20,30], is not expected in our case. Therefore, although we do not have the numerical accuracy to resolve $n > 3$ modes, we can have reasonable confidence that they will be stable. We conclude that by positioning the wall within 1.2 $\times$ the plasma radius this startup sequence becomes stable to all ideal MHD modes.

IV. CONCLUSIONS

We have shown that with the use of current profile control in a low aspect ratio torus we can obtain a high beta tokamak equilibrium that is stable to all ideal MHD modes throughout the entire startup sequence. We maintain high global shear so that one would also expect good stability properties with respect to infernal and tearing modes. The increase in toroidal current at high beta may ameliorate the degradation in energy confinement associated with low current operation.

A conducting wall is required at about 20 % of the minor radius beyond the plasma edge to stabilize low-n modes. The most unstable mode appears to be $n = 3$ which indicates that lower n modes are more strongly stabilized by the wall. We expect higher n modes to be stable since a saturation appears to have set in as indicated by the $n = 3$ mode being only slightly more unstable than the $n = 2$ and since we have shown that high n modes are stable.

The non-ohmic current profile required suggests using second stability in conjunction with steady state operation. The low toroidal current corresponding to high q operation reduces the current drive power requirements, thus making the power balance during current drive more favorable. Bootstrap currents that may appear in high beta equilibria would also reduce the current drive requirements although the profiles produced may not be optimum.

ACKNOWLEDGEMENTS

The authors would like to thank M. Porkolab for important contributions relating to the feasibility of current profile control using rf current drive. We also thank A. Todd (Grumman Aerospace), J. Manickam (Princeton Plasma Physics Laboratory) and P. Hakkarainen for assistance with the numerical codes. Finally we thank B. Lane and J. P. Freidberg for helpful and insightful comments. This work was performed under U.S. Department of Energy contract DE-AC02-78ET51013.

References:

[1] B. Coppi, A. Ferreira, J.W.-K. Mark and J.J. Ramos, Nucl. Fusion **19**, 715 (1979).

[2] C. Mercier, in Plasma Physics and Controlled Nuclear Fusion Research 1978, Proceedings of the 7^{th} International Conference, Berchtesgarden (IAEA, Vienna, 1979), Vol. 1, p. 701.

[3] P.J. Fielding and F.A.Haas, in Plasma Physics and Controlled Nuclear Fusion Research 1978, Proceedings of the 7^{th} International Conference, Berchtesgarden (IAEA, Vienna, 1979), Vol.1, p. 630.

[4] D.Lortz and J. Nuhrenberg, Phys. Lett. **68A**, 49(1978).

[5] H.R. Strauss, W. Park, D.A. Monticello,R.B. White, S.C. Jardin, M.S. Chance, A.M.M. Todd, and A.H. Glasser, Nucl. Fusion **20**, 638(1980).

[6] J.M. Greene and M.S. Chance,Nucl. Fusion **21**, 453 (1981).

[7] T.Antonsen, B.Basu, B. Coppi, G. Crew, R. Englade, A. Ferreira, B. Lane, F. Pegoraro, M. Porkolab, J.J. Ramos, N. Sharky and L. Sugiyama, in Plasma Physics and Controlled Nuclear Fusion Research 1980, Proceedings of the 8^{th} International Conference, Brussels (IAEA, Vienna, 1981), Vol.1, p. 83.

[8] B. Coppi, G.B. Crew and J.J. Ramos, Comments on Plasma Physics and Controlled Fusion, **6**,109(1981).

[9] L. Sugiyama and J.W-K. Mark, Physics Letters, **84**,123 (1981).

[10] B. Coppi, G.B. Crew and J.J. Ramos, Comments on Plasma Physics and Controlled Fusion, **8**,11(1983).

[11] T.Takeda, T. Tsunematsu, T. Tuda, M. Azumi, T. Takizuka, S.Tokuda, G. Kurita, K. Itoh, K. Naraoka, Y. Takaka and S.-I. Itoh, in Plasma Physics and Controlled Nuclear Fusion Research 1982, Proceedings of the 9th International Conference, Baltimore (IAEA, Vienna, 1983), Vol. 3, p. 23.

[12] S. Seki, T. Tsunematsu, M. Azumi, T. Nemato, Nucl. Fus. **27** 330 (1987).

[13] A.M.M. Todd, M. Phillips, M. Chance, J. Manickam and N. Pomphrey, in Plasma Physics and Controlled Nuclear Fusion Research 1986, Proceedings of the 11th International Conference, Kyoto (IAEA, Vienna, 1987), Vol.2, p. 37.

[14] M.S. Chance, S.C. Jardin and T. Stix, Phys. Rev. Letters, **51**, (1983), 1963.

[15] K. Yamazaki, H. Naitou, T. Amano, Y. Hamada, K. Matsuoka, Y. Midzunu, Y. Nakayama, T. Sato, T. Tsunematsu, T. Tuda, S. Seki, M. Azumi, S. Tokuda, T. Ozeki, T. Nemoto, Y. Kishimoto and T. Takeda, in Plasma Physics and Controlled Nuclear Fusion Research 1986, Proceedings of the 11th International Conference, Kyoto (IAEA, Vienna, 1987), Vol. 2, p. 27.

[16] R.C. Grimm, et. al. , Nuclear Fusion,**25** (1985) 805.

[17] M.E. Mauel, Nucl. Fus. **27**, 313 (1987).

[18] G. Navratil, Y. Baransky, A. Bhattacharjee, C.K. Chu, A.V. Deniz, A.A. Grossman, A. Holland, T. Ivers, X.L. Li, T.C. Marshall, M.E. Mauel, S. Sabbagh, A.K. Sen, J. Van Dam, X.-H. Wang, M. Hughes, M. Phillips and A.M.M. Todd in Plasma Physics and Controlled Nuclear Fusion Research 1986, Proceedings of the 11th International Conference, Kyoto (IAEA, Vienna, 1987), Vol. 1, p. 299.

[19] H. Naitou, J.W. Van Dam, D.C. Barnes, Nucl. Fus. **27**, 765 (1987).

[20] J. Manickam, N. Pomphrey, and A.A.M. Todd, Nucl. Fusion **27**, 1461 (1987).

[21] R.C.Grimm, R.L.Dewar, and J.Manickam, J. Comp. Physics **4**, 94 (1983).

[22] B. Coppi, Physics Review Letters **39**, 939(1977).

[23] D. Dobrott, D.B. Nelson, J.M. Greene, A.H. Glasser, M.S. Chance and E. A. Frieman, Physics Review Letters **39**, 943 (1977).

[24] J.W. Connor, R.J. Hastie and J.B. Taylor, Physics Review Letters **40**, 396 (1978).

[25] F. Bauer, O. Betancourt and P. Garabedian, Phys. Fluids **24**, 48(1981).

[26] G. B. Crew and J.J. Ramos, Phys. Rev. **26A**, 1149(1982); Phys. Fluids **26**, 2621 (1983).

[27] S. Tokuda, T. Tsunematsu, M. Azumi, T. Takizuka and T. Takeda, Nucl. Fusion **22**, 661(1982).

[28] J. Manickam, Nucl. Fusion **24**, 595 (1984).

[29] V.D. Shafranov in Reviews of Plasma Physics (Consultants Bureau, Plenum Publishers, New York, 1966) Vol. 2, p. 103.

[30] R.J.Hastie and J.B.Taylor, Nucl. Fusion **21**, 187 (1981).

[31] F.Troyon, R.Gruber, H. Suarenmann, S. Semenzato and S. Succi, Plasma Physics and Controlled Fusion **26**, 209 (1984).

Table I

Tokamak parameters

Aspect Ratio	3
q_0	2
q_e	7.6
Minor Radius (m)	0.3
Ellipticity, κ	1.4
Triangularity, δ	0.3
Vacuum Toroidal Field (T)	1
Plasma Current (kA)	130-280

FIGURE CAPTIONS

1. Schematic indicating distortion of field lines at high beta in $\phi - \theta$ space. Also shown (dashed line) is the normal curvature as a function of θ.

2. Schematic indicating distortion of integrated local shear, I, at high beta. Curve marked $\theta_0 \neq 0$ contains integration constant appropriate to the most unstable eigenmode. Dashed curve indicates geodesic curvature.

3. Contours of constant local shear for tokamaks with $q_0 = 2$ and $q_e = 7.6$. a) A=20 and $\beta_p = 0.01$, b) A=3, $\beta_p = 0.01$ c) A=3, $\kappa = 1.4$, $\delta = 0.3$, $\beta_p = 0.01$, d) A=3, $\kappa = 1.4$, $\delta = 0.3$, $\beta_p = 1.4$. The cross-hatched region contains negative local shear.

4. Poloidal flux contours for four characteristic equilibrium states in our $q_0 = 2$ sequence. The corresponding equilibrium poloidal betas are a) $\beta_p = 0.2$, b) $\beta_p = 1.25$, c) $\beta_p = 2$, d) $\beta_p = 3.1$ and the volume averaged total betas are a) $\beta = 0.06\%$, b) $\beta = 0.61\%$, c) $\beta = 1.41\%$, d) $\beta = 3.40$ % .

5. Toroidal current contours for the four equilibria displayed in Fig. 4.

6. Ohmic current (arbitrary units) vs. flux for the four equilibria displayed in Fig. 4.

7. Safety factor q vs. flux for for the four equilibria displayed in Fig. 4.

8. Plasma pressure p, safety factor q, toroidal field and toroidal current j_ϕ , vs. major radius at the torus midplane for $\beta = 10.8$ %.

9. High-n ballooning mode stability factor (on least stable flux surface) vs. β_p for equilibria characterized by $q_0 = 1$ $q_e = 4$, $q_0 = 1.5$ $q_e = 6$, and $q_0 = 2$ $q_e = 7.6$.

10. q_0 value required for a stable transition into the second stability region as a function of the aspect ratio, A. q_e is fixed at 8.

11. Wall location required for marginal stability of q_0=2 equilibria against low-n modes. $n = 1$, 2 and 3 modes are shown.

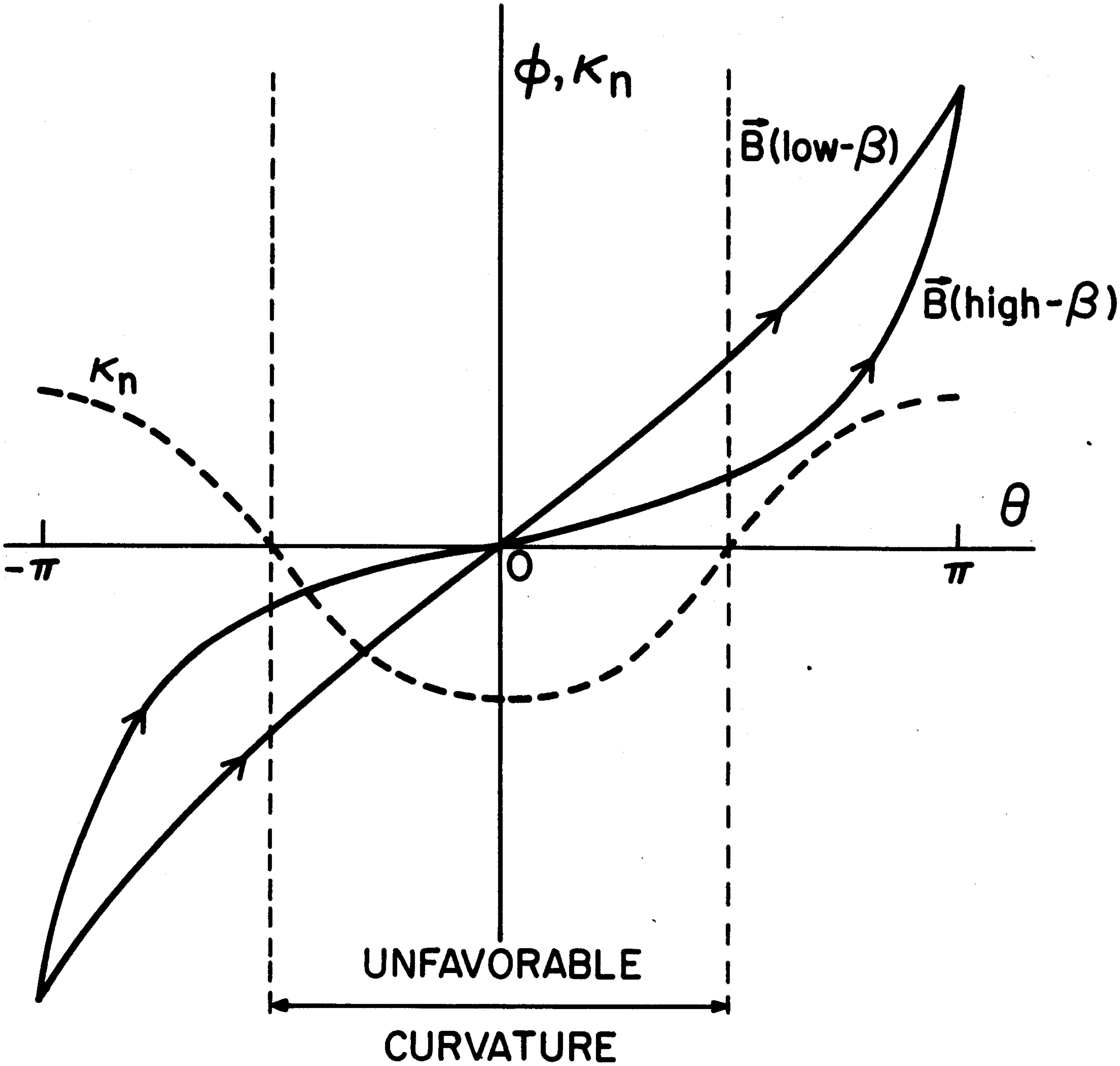

φ, κn
B(low-β)
B(high-β)
κn
θ
-π
0
π
UNFAVORABLE
CURVATURE

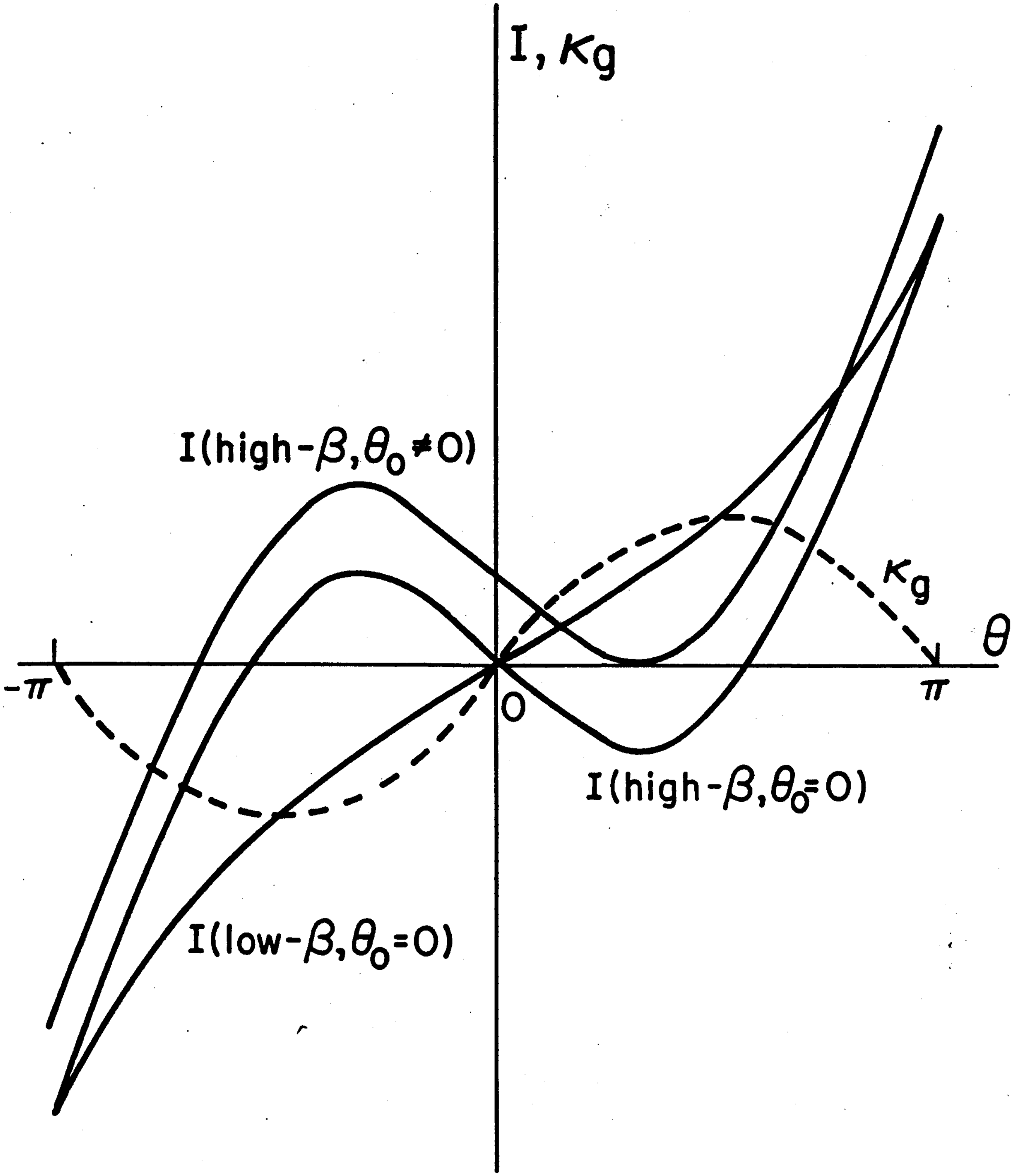

I, κg
I(high-β, θ0≠0)
κg
θ
-π
π
0
I(high-β, θ0=0)
I(low-β, θ0=0)

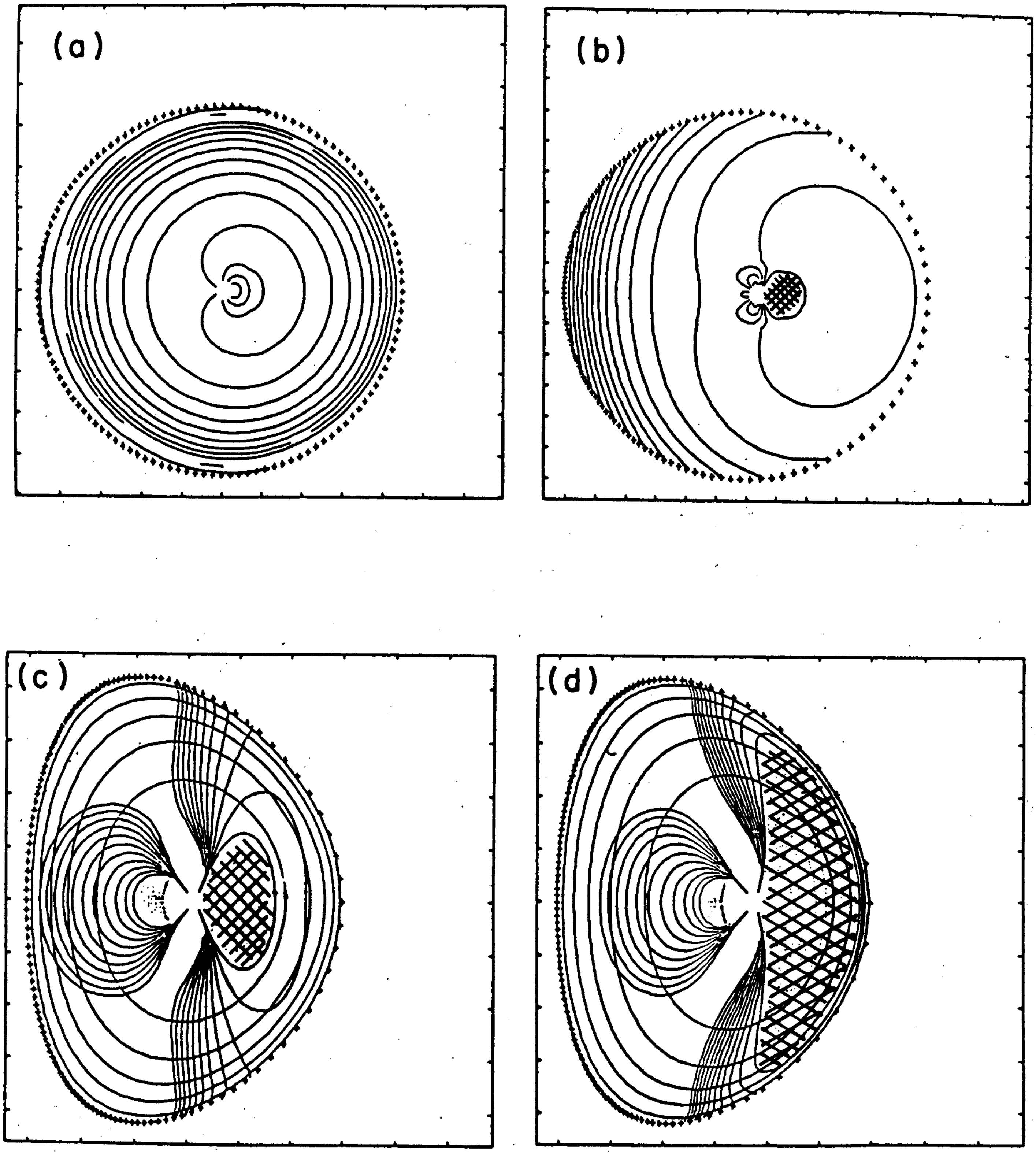
(a)
(b)
(c)
(d)

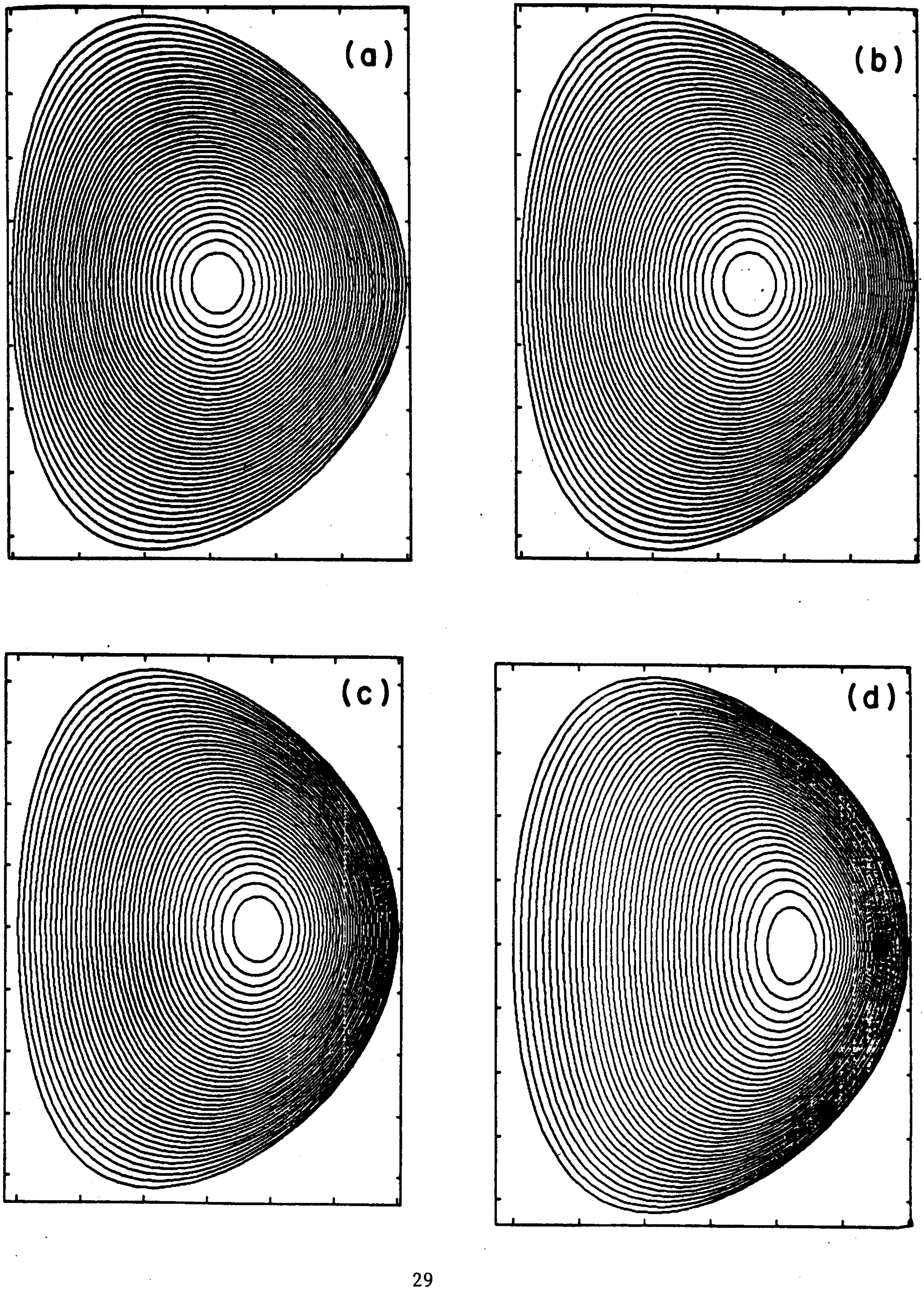
(a)
(b)
(c)
(d)

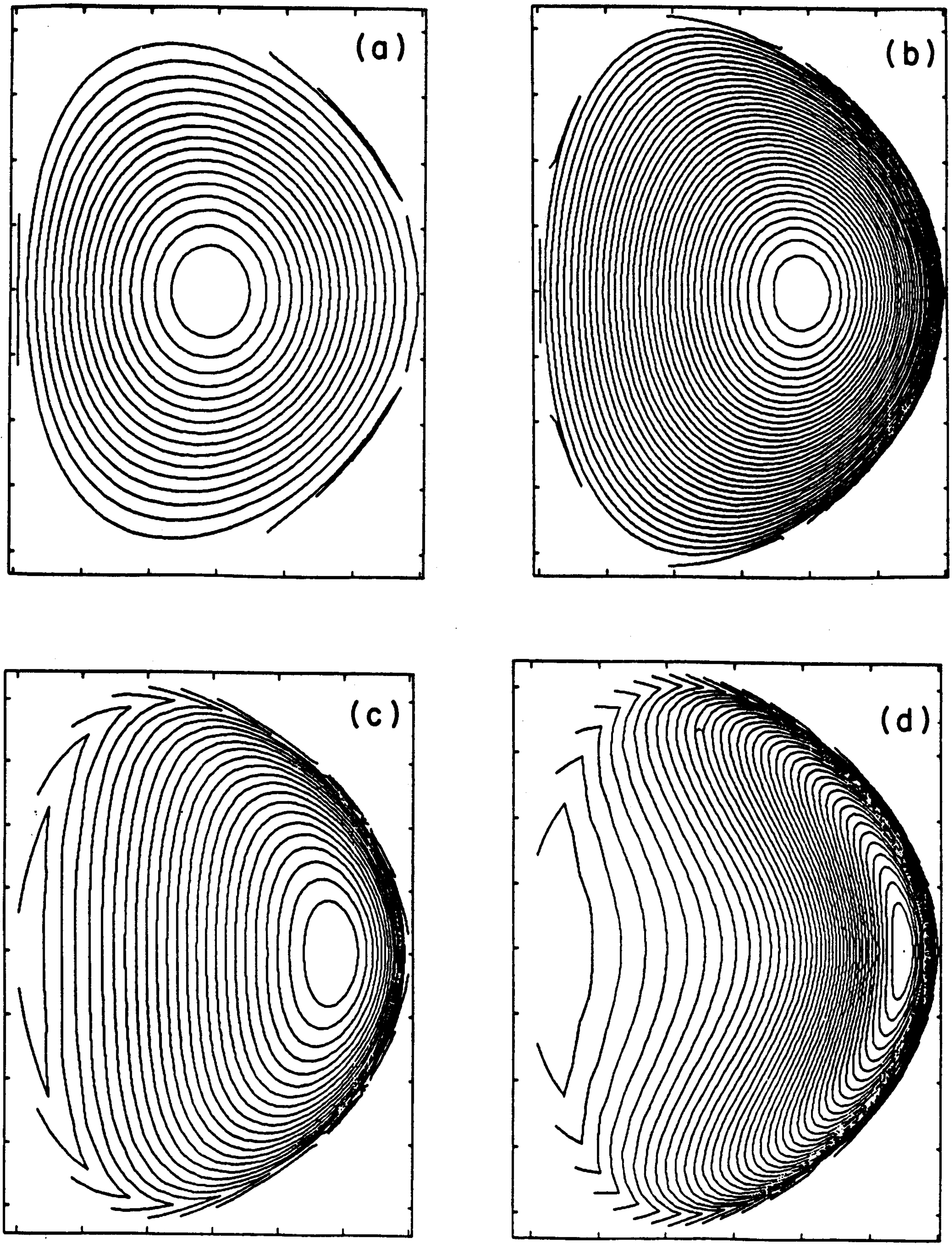

(a)
(b)
(c)
(d)

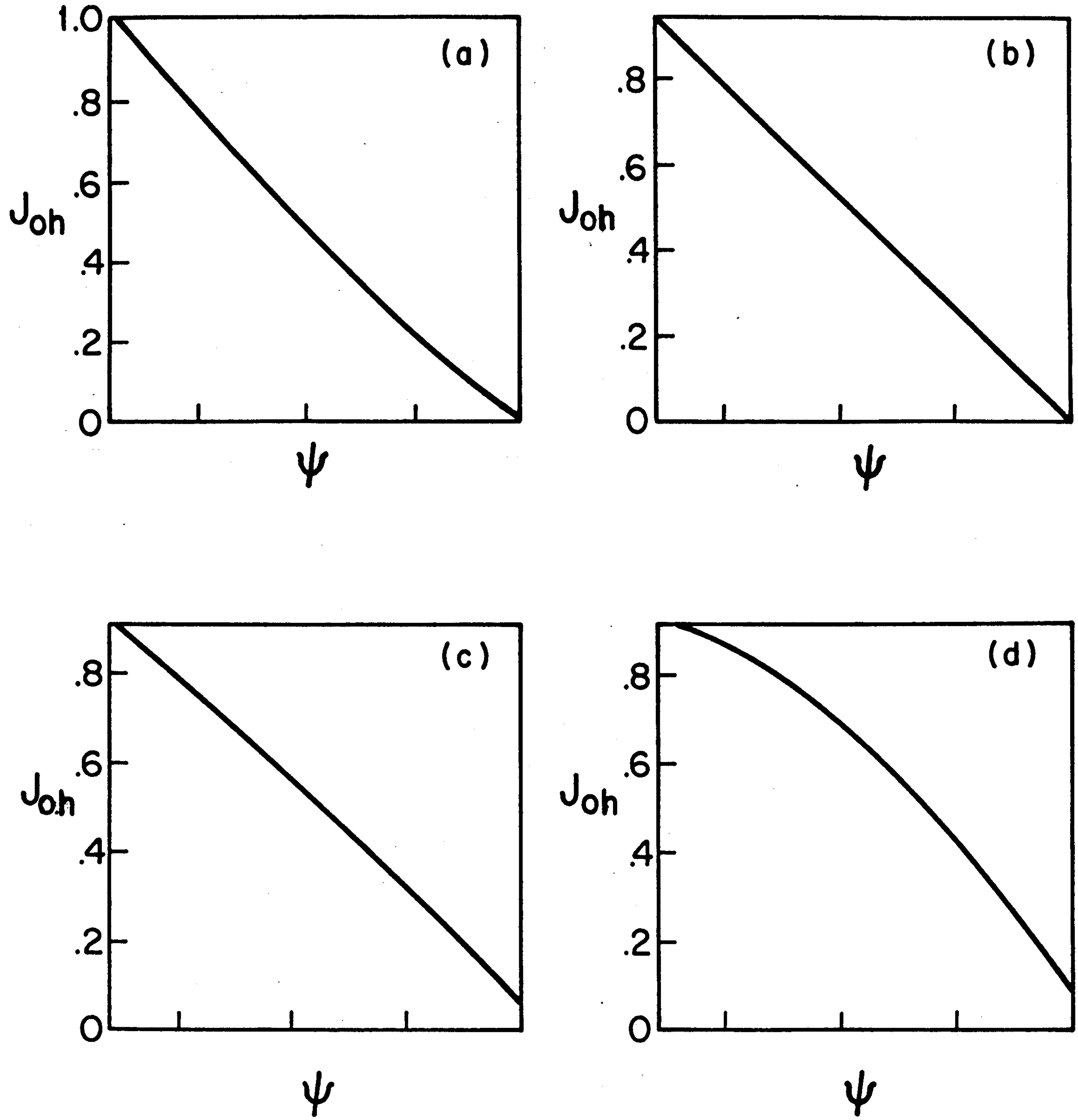

(a)
1.0
.8
.6
.4
.2
0
J_{oh}
ψ
(b)
.8
.6
.4
.2
0
J_{oh}
ψ
(c)
.8
.6
.4
.2
0
J_{oh}
ψ
(d)
.8
.6
.4
.2
0
J_{oh}
ψ

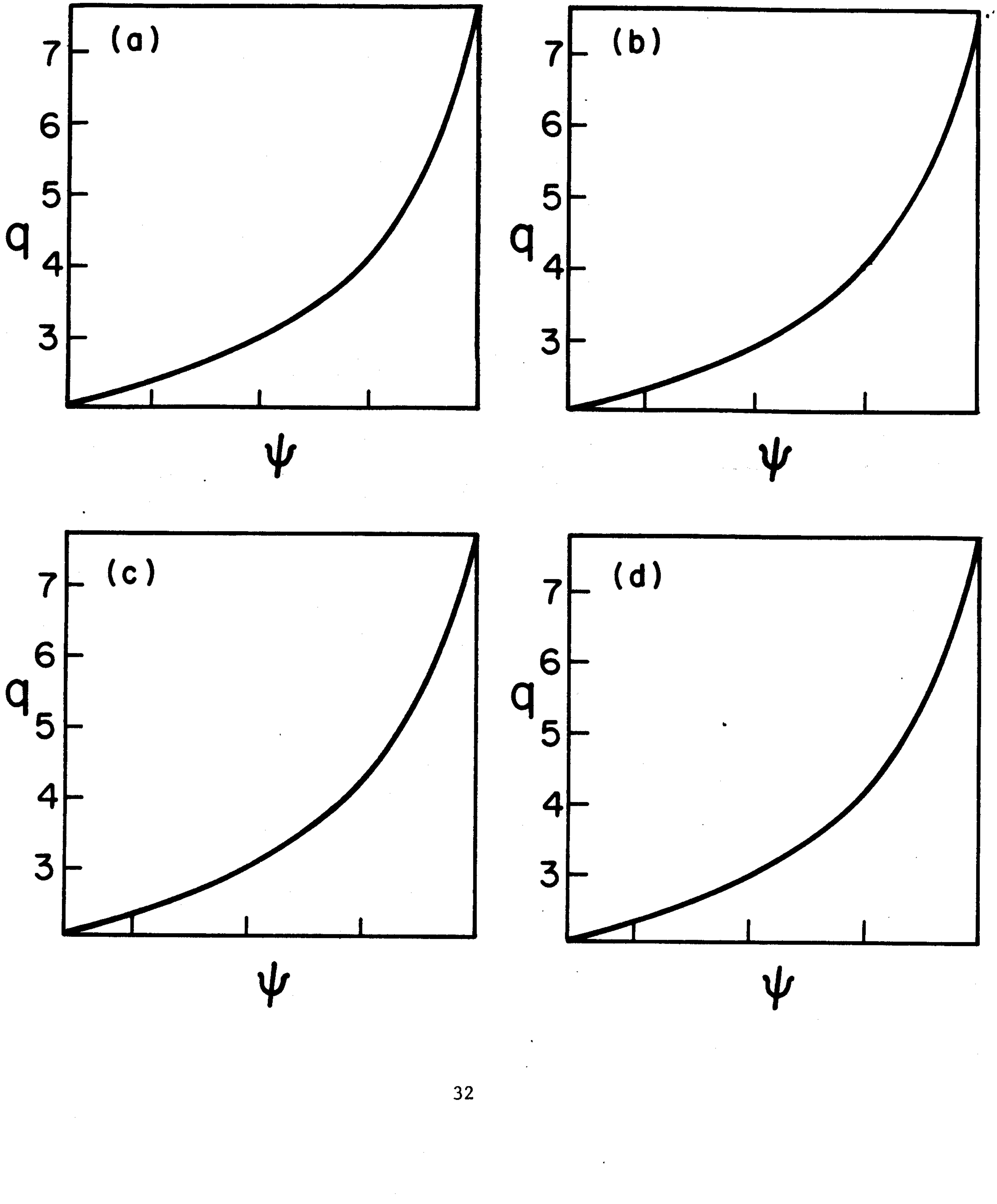

(a)
(b)
(c)
(d)
q
ψ
3
4
5
6
7

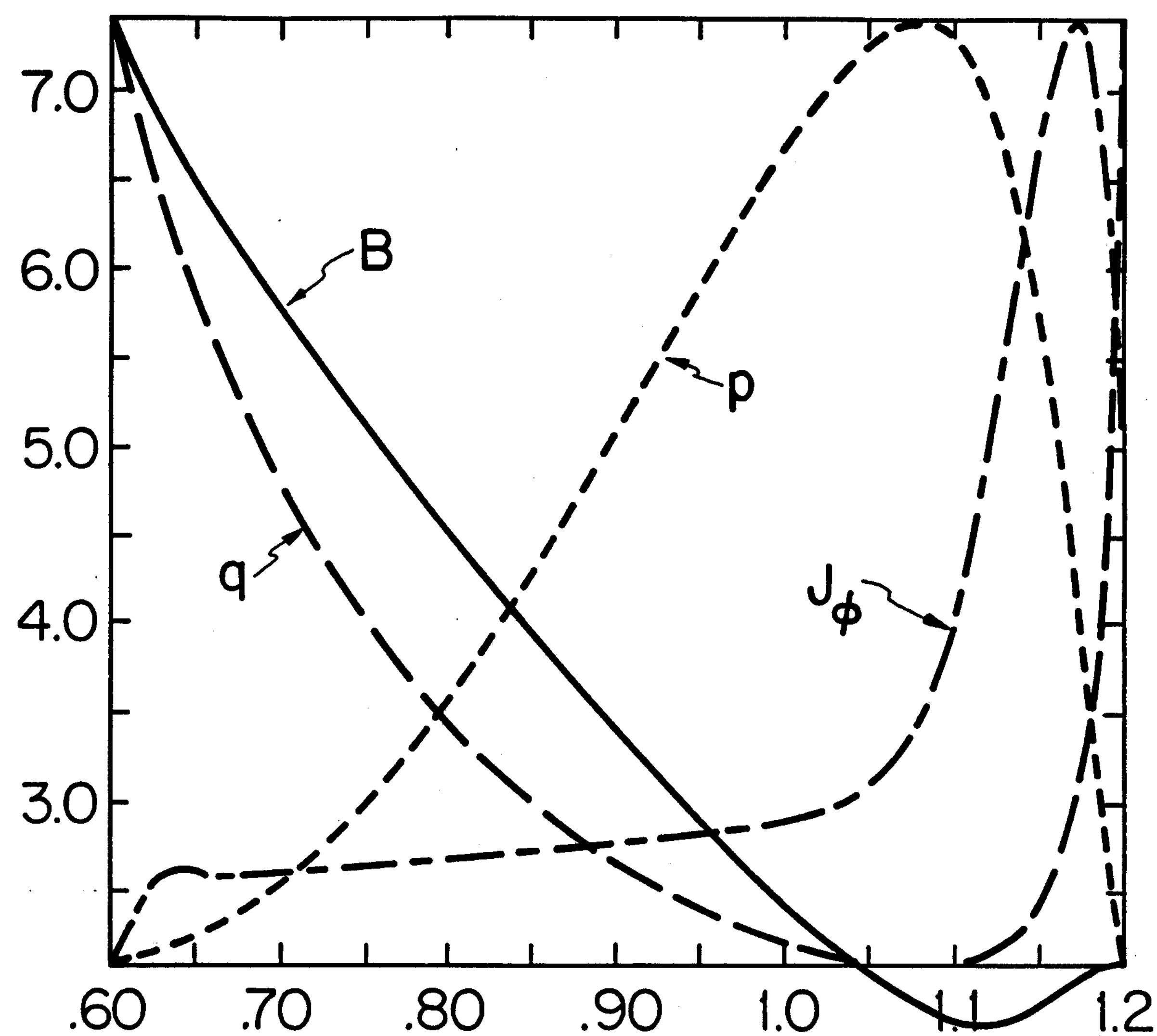

7.0
6.0
5.0
4.0
3.0
.60
.70
.80
.90
1.0
1.1
1.2
B
p
q
J_ϕ

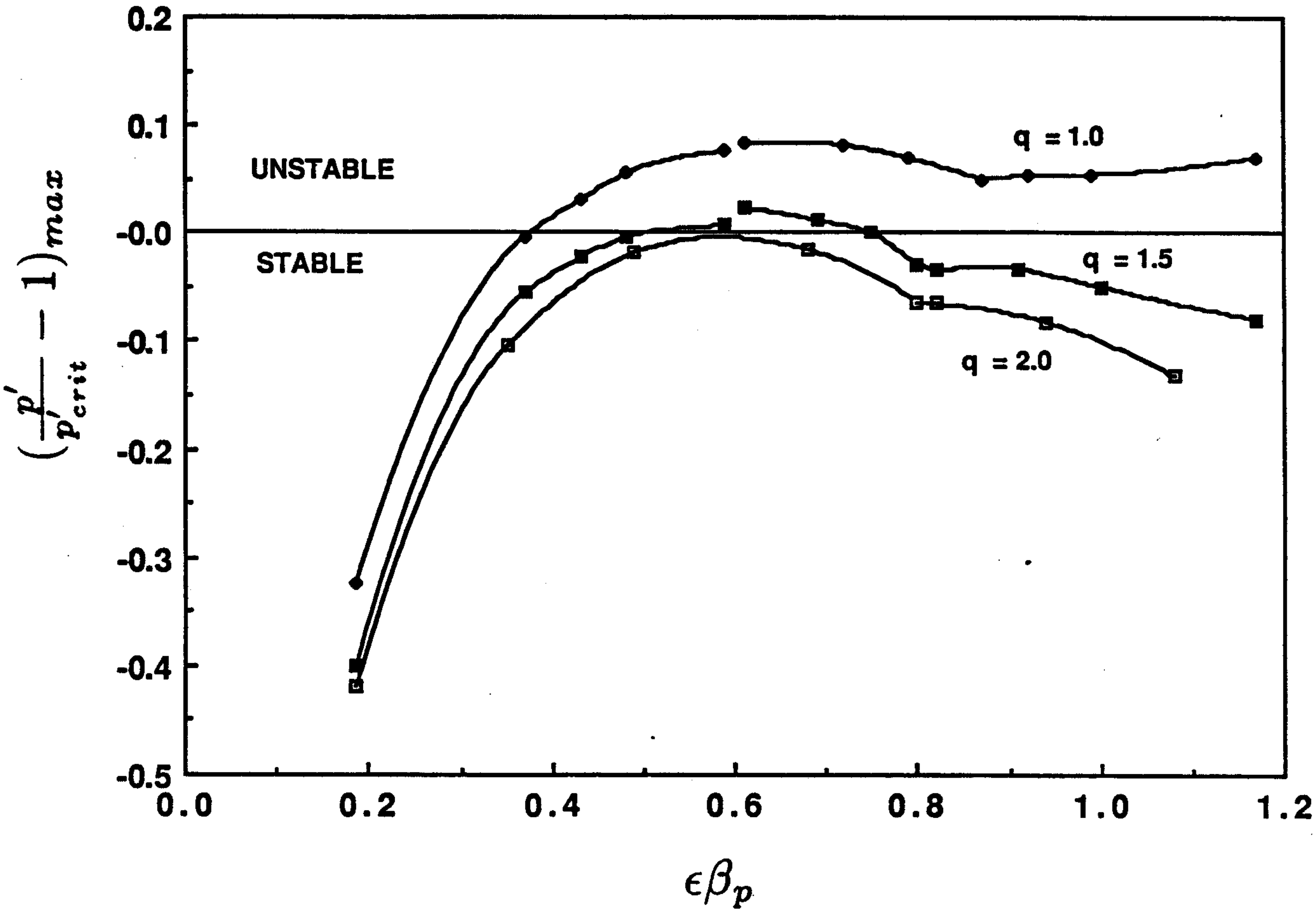

0.2
0.1
-0.0
-0.1
-0.2
-0.3
-0.4
-0.5
0.0
0.2
0.4
0.6
0.8
1.0
1.2
UNSTABLE
STABLE
q = 1.0
q = 1.5
q = 2.0
$(\frac{p'}{p'_{crit}} - 1)_{max}$
$\epsilon\beta_p$

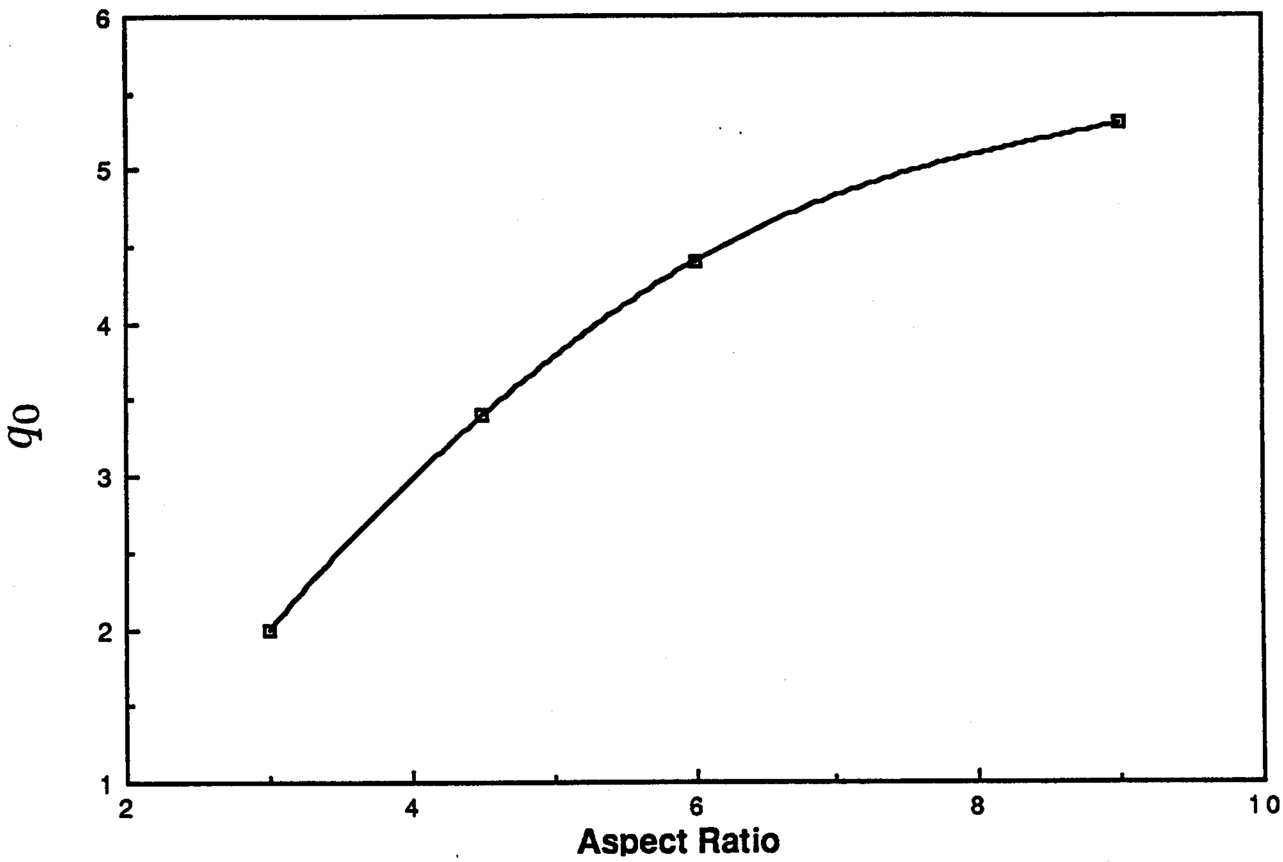
6
5
4
3
2
1
q0
2
4
6
8
10
Aspect Ratio

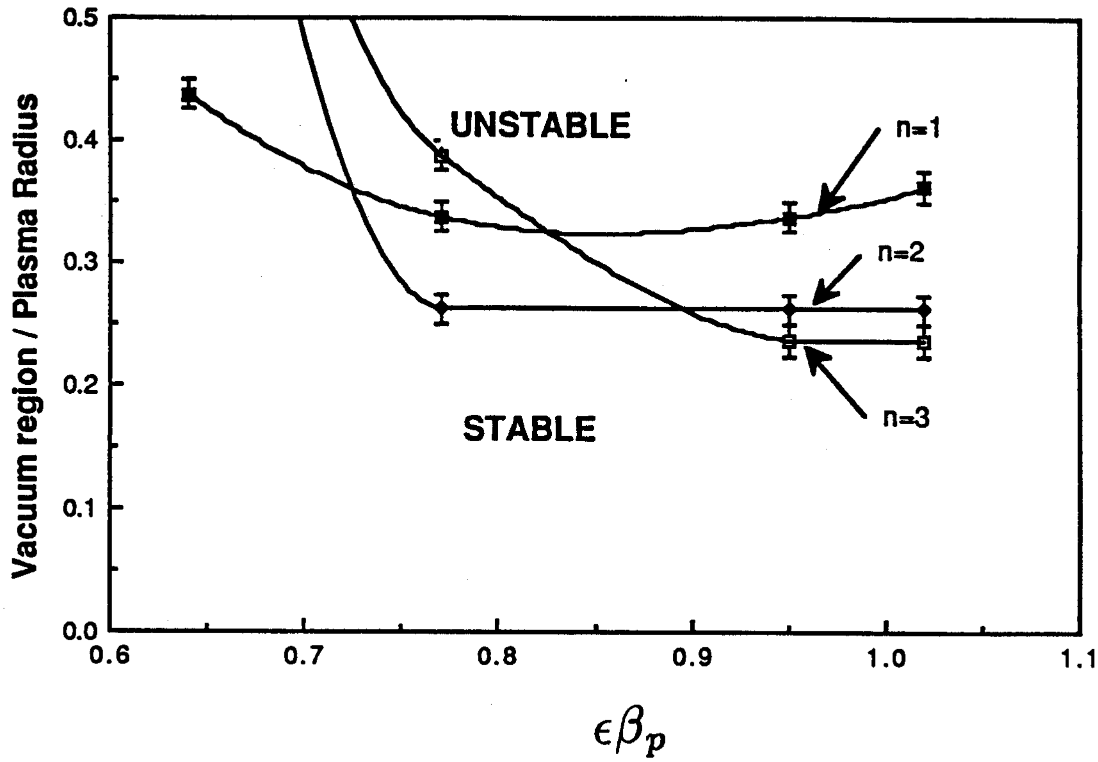

0.5
0.4
0.3
0.2
0.1
0.0
0.6
0.7
0.8
0.9
1.0
1.1
Vacuum region / Plasma Radius
UNSTABLE
STABLE
n=1
n=2
n=3
$\epsilon\beta_p$